



## Removal of benzothiophene and dibenzothiophene from hydrocarbon fuels using CuCe mesoporous Y zeolites in the presence of aromatics

Kevin X. Lee<sup>a</sup>, George Tsilomelekis<sup>b</sup>, Julia A. Valla<sup>a,\*</sup>

<sup>a</sup> Department of Chemical and Biomolecular Engineering, University of Connecticut, Storrs, CT 06269, USA

<sup>b</sup> Department of Chemical and Biochemical Engineering, Rutgers University, Piscataway, NJ 08854, USA



### ARTICLE INFO

#### Keywords:

Mesoporous Y  
Sulfur adsorption  
Bimetallic  
Metal-exchanged mesoporous Y  
Desulfurization

### ABSTRACT

Adsorptive desulfurization of sulfur compounds in transportation fuels, such as benzothiophenes from gasoline and jet fuels and dibenzothiophenes from diesel, can be inhibited by diffusion limitations in porous materials as well as the presence of aromatic hydrocarbons. In this study we demonstrate that adsorptive desulfurization using bimetal-exchanged mesoporous Y zeolites can overcome these challenges without sacrificing high sulfur adsorption capacity. The mesopores shorten the diffusion path length toward the internal active sites of the zeolite, while the metals (in this study Ce and Cu), not only create relatively stronger bonds, but also multiple adsorption configurations. The bimetallic mesoporous Y zeolites were prepared using a templated top-down approach, followed by the introduction of the metals, Cu and Ce, via ion-exchange. The ability of each zeolite to remove sulfur compounds is demonstrated by fixed-bed experiments. Model fuels were prepared using benzothiophene and dibenzothiophene in octane, benzene and naphthalene. The adsorption mechanisms of benzothiophene and dibenzothiophene were further studied, at the molecular level, using in-situ Diffuse Reflectance Infrared Fourier Transform Spectra (DRIFTS). Our results indicate that the metals display high affinity for the aforementioned sulfur compounds, via either  $\pi$ -complexation or  $\sigma$ -bond interaction. Specifically, Ce-exchanged Y zeolites exhibit multiple adsorption modes, as they can adsorb the sulfur compounds via the both configurations. Furthermore, the mesoporosity in Y zeolites enable the adsorption of dibenzothiophene with a diffusion coefficient of 4.5x greater than the parent Y zeolite. In conclusion, bimetallic mesoporous Y zeolites exhibited DBT capacity of almost 50 mL/g, five times more than parent Y, due to both improved mass transfer and high adsorption energy.

### 1. Introduction

Recent decline in crude oil price has reinforced the utilization of processed fuels in various sectors such as industrial, infrastructure, commercial and transportation [1]. The 55% drop in oil price since 2013 sees a consequential decrease in the price of processed fuels, such as commercial gasoline, diesel fuel and jet fuel as seen in Fig. 1 [2]. Furthermore, the discovery of new oil reserves promotes interest in the utilization of fossil-based fuels, especially in the transportation sector [3]. Hence, while renewable energy (e.g. based on biomass resources [4,5]) is still receiving considerable attention, adequate supply and reasonable cost of fossil-based fuels inevitably promote the production of gasoline and diesel. The increasing demand in fossil-based fuels, however, quickly become a global concern when lethal emissions into the atmosphere are taken into account. According to the Environmental Protection Agency (EPA), transportation fuels contribute about 50% of nitrogen oxide ( $\text{NO}_x$ ) and 5% of sulfur oxide ( $\text{SO}_x$ ) emitted annually

[6,7]. The  $\text{SO}_x$  emission may seem insignificant, but it has been proven that only a small amount of sulfur contamination, could lead to catalytic converter failures or even fuel cell electrode poisoning [8,9]. If sulfur levels are not properly monitored, traces of sulfur oxides can impede the activity of automotive catalysts and electrocatalysts by altering the surface properties and consequently, influencing the efficiency and activity of the catalysts [10]. Without proper implementation of sulfur removal mechanism, the emitted  $\text{SO}_2$  can react with water vapor in the atmosphere to form sulfuric acid, which is one of the precursors of acid rain [11,12].

To prevent this growing problem, the EPA has introduced mandatory transportation fuel regulations, which limit the sulfur concentrations in gasoline and diesel fuel to 10 and 15 ppmw, respectively [13]. While the aforementioned sulfur standards may be attainable by conventional desulfurization methods, fuel cell membranes require their electrolytes to contain less than 1 ppmw of sulfur [11,12]. Furthermore, refractory sulfur compounds in diesel fuel such as alkyl-

\* Corresponding author.

E-mail address: [ioulia.valla@uconn.edu](mailto:ioulia.valla@uconn.edu) (J.A. Valla).

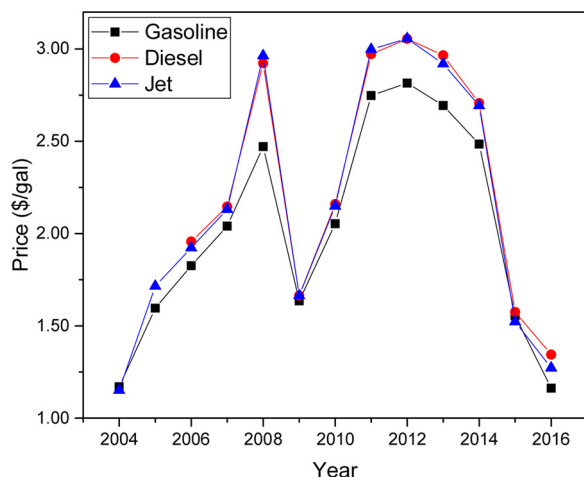


Fig. 1. Prices of Petroleum Products since 2004 [2].

dibenzothiophenes compounds are very stable, rendering the cleavage of C–S bond impossible without involving excessive energy. Due to their refractive and abundant nature, considerable amount of sulfur compounds can still be found in fuels after the fluid catalytic cracking (FCC) process [14–16]. Conventional hydrodesulfurization (HDS) is widely used in the refinery to remove sulfides, mercaptans and thiophenes. The recent advancement of HDS catalyst has also enabled the catalytic conversion of larger sulfur compounds such as dibenzothiophene (DBT) to  $\text{H}_2\text{S}$  either via direct desulfurization or hydrogenation pathway [17,18]. HDS, however, lacks the capability to produce zero-level sulfur fuels without the use of energy-intensive conditions, such as high pressure and hydrogen consumption. At these severe conditions, excessive hydrogenation of aromatics and olefins in fuels negatively affects other properties of fuel, such as Research Octane Number (RON) [1].

Absorptive desulfurization can be a promising alternative or complementary technology to HDS, because it has the potential to be regenerative, cost-effective, and environment-friendly, while operating at ambient conditions. The streamlined design and synthesis of such adsorbents can render sulfur removal rational towards intensified on-purpose technologies. The utilization of zeolites as liquid-phase sulfur adsorbents is receiving significant attention lately, as they have shown to be very effective in gas-phase sulfur removal in the 1990s [19–21]. As a result, the synthesis and modification of novel adsorbents have received considerable attention in absorptive desulfurization. Among the widely discovered sulfur-selective adsorbents [22–27], faujasite (FAU) Y zeolite has shown to be a promising sorbent material due to the unique 3-dimensional (3D) pore structure and available active (acid) sites. The average-sized micropores of 7.4 Å and inter-connecting sodalite cages allow only certain molecules to access the internal active sites located in their supercage [28]. The highly dense Brønsted acid sites (BAS) act as an adsorption platform by donating proton to nearby adsorbate molecules. While this is highly advantageous in the removal of small molecules in various adsorption applications [29–34], the microporosity of Y zeolites may restrict the transport of refractory sulfur compounds with large kinetic diameter, such as dibenzothiophene (DBT) and other alkyl-branched dibenzothiophenes. Moreover, competitive adsorption imposed by the presence of aromatics, such as benzenes and naphthalenes in gasoline and diesel fuel, respectively, can also impede the selectivity of sulfur compounds. Thus, the overall desulfurization performance could be significantly compromised. These challenges can altogether cause a major drawback in the effort to meet federal sulfur standards assigned by the EPA [13].

It is clear that the aforementioned challenges must first be apprehended before absorptive desulfurization can become an industrially viable technology. The physical and chemical properties of Y zeolite can

be easily altered by tuning the Si/Al ratio either via desilication or dealumination techniques [28]. Furthermore, the relatively high amount of protons in acidic Y zeolites makes them ideal materials for ion-exchanging metal cations. Many research groups have taken various steps to modify the Y zeolite using different state-of-art techniques, such that the mass-transfer resistance and selectivity limitations of the parent material can be overcome. One approach to minimize diffusion limitations is by introducing mesopores via a bottom-up synthesis or a top-down modification [28]. Mesoporous materials with pores ranging from 2 to 50 nm have been extensively studied and utilized for various applications, especially in catalysis [35–38]. More recently, mesoporous zeolites have proven to be promising sorbents in the desulfurization of liquid fuels. Tian et al. investigated the sulfur removal from model fuel containing various thiophenic compounds and found that desilicated H-beta zeolite removes about twice as much total sulfur, compared to the parent beta zeolite [39]. In relation to this, the Wang group suggested that the sulfur capacity of jet fuel increases by three-fold with the large pore SBA-15 compared to the parent zeolite [40]. A similar result was also observed by Yang et al. as mesoporous materials, such as SBA-15 and MCM-41, improved the mass transfer of sulfur compounds to the adsorption sites, when used as supports [41]. While the introduction of larger pores may improve the kinetics of these larger molecules, the role of adsorption equilibrium on the overall desulfurization performance should not be completely ignored. The introduction of mesopores will inevitably cause a partial loss of active sites responsible for adsorbing sulfur. One effective way to introduce mesoporosity without sacrificing too much microporosity, is by using a hydrophobic mesopore-template as demonstrated by Li et al. [42]. They synthesized mesoporous aluminosilicate (MAS) using cetyltrimethylammonium bromide (CTAB) as a directing agent and discovered that it exhibits 20% higher sulfur adsorption capacity compared to NaY and MCM-41 for the desulfurization of diesel. Furthermore, as demonstrated by Oliver and co-workers [25], the pore size optimization of silica-zirconia templated by dodecylamine (DDA) allows for better sorbent regenerability and higher adsorption capacity of  $12.4 \text{ mgS g}^{-1}$  compared to its counterpart templated by the longer hexadecylamine (HDA).

As previously discussed, the introduction of mesoporosity may inevitably remove some internal active sites responsible for sulfur adsorption. This loss can be replenished by incorporating active metal cations with high sulfur affinity. The role of metals in the selective adsorption of sulfur has been studied in the past. Yang and colleagues were pioneering founders of the strong  $\pi$ -complexation sorbents [43]. They conducted gas-phase desulfurization experiments and molecular orbital calculations on CuY and AgY in the presence of thiophene and benzene, and showed that the materials exhibited higher adsorption capacity compared to NaY. These promising results allowed the Yang group to extend the excellent performance of  $\pi$ -complexation sorbents, as well as other newly developed sorbents, such as NiY and ZnY, toward liquid-phase desulfurization, with CuY reporting the highest sulfur capacity [26,44–47]. The  $\pi$ -type interaction displays convincing capacity of sulfur, however, becomes ineffective if competing additives are present in the fuel [48]. Song et al. realized this potential drawback and proposed  $\sigma$ -forming sorbents that can adsorb thiophenes more selectively via the direct  $\sigma$ -bond [48,49]. They showed that NiY was able to adsorb 1.7 times more sulfur from commercial gasoline compared to CuY, which led them to explore other high positive charge cations including f-block elements, such as Ce that have the tendency to complex with the S atom directly. The selective nature of  $\sigma$ -type sorbents has been confirmed by other groups in different desulfurization studies [50–52]. In a similar work, LaHUSY was used to selectively remove BT and DBT in the presence of naphthalene [53], which demonstrates the ability of lanthanides to form two types of bonding with the sulfur compounds. Yang et al. also investigated the effect of both naphthalene and benzene on the removal of BT using modified activated carbons [54].

In our previous work [55], we introduced a novel desulfurization sorbent that exhibits high sulfur capacity with low mass transfer resistance. The metal-exchanged mesoporous Y zeolites contained hierarchical pores designed to eliminate diffusion limitations, while keeping an adequate amount of internal active sites for sulfur adsorption. Commercial fuels contain various types of organic compounds, and thus their role in adsorptive desulfurization must not be neglected. In this study, we rationally introduced bimetallics into our hierarchical zeolites to further enhance the selective adsorption of sulfur compounds from a model fuel mixture. The utilization of bimetallic systems on adsorption has yet to be fully understood, as only limited studies of metal combinations exchanged in zeolites have been reported. Song and co-workers found that CuCeY displayed a 3-fold increase in adsorption capacity of model gasoline compared to CuY [27]. They proposed that this improvement was due to the synergistic interaction between Cu and Ce. Wang et al. have demonstrated that the desulfurization performance of NiCeY in removing DBT from a feed of 5% toluene and 95% octane, is higher compared to the performance of NiY and CeY [56]. More recently, a group from Northeast Petroleum University in China presented encouraging results on deep adsorptive desulfurization using bimetal-exchanged Y zeolites [57,58]. They showed that in both batch and fixed-bed adsorption, CuCeY can adsorb more sulfur from a model fuel containing toluene or cyclohexane via the  $\pi$ -complexation and S–M bond interactions compared to the monometallic counterpart. With benzothiophene (BT) being the biggest sulfur compound tested, the breakthrough point was extended by at least 50 mL/g and 30 mL/g on CuCeY compared to CeY and CuY, respectively. To the best of our knowledge, there are no studies on the adsorptive desulfurization performance of bimetal-exchanged mesoporous Y zeolites in a mixture of aromatics. Hence, the current work highlights the role of metals, bimetallics (Cu and Ce) and mesoporosity in Y zeolites on the desulfurization of model fuels, containing benzothiophene and dibenzothiophene, in a fixed-bed adsorber. The influence of benzene and naphthalene as a competing aromatic in the fuel has been tested. Mechanistic studies have also been performed to correlate the mechanism of sulfur adsorption to each metal-exchanged zeolite.

## 2. Materials and Methods

### 2.1. Preparation of bimetal-exchanged mesoporous Y zeolites

CBV300 ( $\text{NH}_4\text{Y}$ ) was obtained from Zeolyst International and used as starting material. The preparation of mesoporous Y was conducted using the surfactant-assisted (SA) method developed by Garcia-Martinez et al. [28,59]. Metal-exchanged mesoporous Y was prepared by first tailoring the mesoporous Y, followed by ion-exchange using either Ce or Cu nitrate precursors to make CeSAY or CuSAY, respectively. The mesoporous Y zeolite is labeled as “SAY.” The procedure and conditions have been described in our previous work [55]. To prepare bimetal-exchanged CuCeY or bimetal-exchanged CuCeSAY, the zeolites were first ion-exchanged with Ce nitrate precursor due to higher ion-exchange selectivity, followed by ion-exchange with Cu nitrate precursor [60]. Ce exhibits higher ion-exchange selectivity to replace protons in the zeolite extra-framework, thus should be introduced first prior to Cu [61,62]. Both SAY and metal-exchanged zeolites were calcined at 525 °C to evaporate undesired organics.

### 2.2. Reagents

Three model fuels were prepared: 1) reagent grade *n*-octane + 20 wt% benzene; 2) reagent grade *n*-octane + 1% naphthalene; 3) reagent grade *n*-octane + 1% methyl-naphthalene, to simulate commercial jet and diesel fuels, respectively [63,64]. While it is evident that the concentration of benzene in federal gasoline is about 1 wt% [65], 20 wt% of benzene was used to make consistent comparisons with published results [40,66], while the concentrations of naphthalene and

methyl-naphthalene were maintained at federal levels. The aforementioned model fuels were spiked with 100 ppmw of benzothiophene (BT) and 100 ppmw of dibenzothiophene (DBT). All the chemicals and reagents were purchased from Sigma Aldrich.

### 2.3. Material characterization

Transmission electron microscopy (TEM) studies were carried out in a FEI Talos F200X microscope operating at 200 kV. The instrument is equipped with an X-FEG field emission source and a super X-EDS system. A small amount of zeolite suspended in ethanol was deposited onto a carbon-film copper grid. Once the ethanol has been evaporated, the copper grid was placed into the TEM to observe the crystallinity and porosity of the zeolites, as well as the presence of metal nanoparticles. Surface area, pore volume and surface structure of the materials, which had been outgassed at 120 °C, were characterized using a Micromeritics ASAP 2020 analyzer and the data were analyzed based on the Brunauer, Emmett and Teller (BET) method. The bulk content of metals in the zeolites were determined using an inductively coupled plasma with a mass spectrometer (ICP-MS). The reduction conditions of the materials were characterized by temperature-programmed reduction (TPR) in 3%  $\text{H}_2$  using a PerkinElmer Pyris 1 thermogravimetric analyzer (TGA). Each material was subjected to a temperature ramp from 50 °C to 1000 °C at a rate of 5 °C/min, and the temperature at which the weight loss occurs was recorded, while the amount of  $\text{H}_2$  consumed was used to estimate the metal content.

### 2.4. Fixed-bed adsorption experiment

All adsorption-breakthrough experiments were conducted in a custom-made quartz column with an outside diameter of  $\frac{1}{4}$ " and a height of 26 cm. The column was packed with 0.2–0.3 g of zeolite powders until a consistent height of 3 cm has been reached. Prior to each adsorption experiment, the column containing the packed-bed of metal-free zeolites was activated at 450 °C for 2 h under constant  $\text{N}_2$  gas flow. Metal-containing zeolites were activated in  $\text{H}_2$  gas at the same conditions as above. After activation, the column was allowed to cool under flowing  $\text{N}_2$  or  $\text{H}_2$  to prevent contact with air. Next, the model fuel was allowed to flow through the packed bed at 0.05 mL/min flow rate. A gas-chromatograph (GC) vial was placed right below the column exit to collect 0.5 mL of effluent droplets at consistent time intervals. The collected effluents were transferred to a GC system equipped with a sulfur chemiluminescence detector (G C-SCD) for analysis of sulfur content, and the collected data was used to construct a breakthrough curve.

### 2.5. Adsorptive mechanistic studies by infrared spectroscopy

Diffuse Reflectance Infrared Fourier Transform Spectra (DRIFTS) were collected using a Nicolet 6700 Fourier transform infrared (FTIR) spectrometer equipped with a DRIFT cell made by Harrick Scientific and ZnSe window dome. Each spectrum was recorded using 32 scans with a resolution of  $4 \text{ cm}^{-1}$  at increments of 50 °C from 100 °C to 500 °C for BT and from 200 °C to 500 °C for DBT. The FTIR spectrometer was connected to a stainless steel line, mass flow controllers and an Edwards T-Station 75 turbomolecular vacuum pump to allow *in-situ* study of sulfur adsorption and desorption. About 20–30 mg of zeolite powder was loaded into the DRIFT cell and degassed at 450 °C under  $\text{N}_2$  or  $\text{H}_2$  flow for 2 h. After being cooled down to 100 °C, BT vapor was introduced from a reservoir onto the zeolite and allowed to adsorb for about 10 min until saturation was achieved. After adsorption, the sample was purged, evacuated and then subjected to temperature-programmed desorption (TPD) until the regeneration of the original sample was observed. As for DBT, the sulfur solids were added directly to the sample after cooling and allowed to adsorb at 200 °C, followed by the same desorption steps described above. The analysis of all spectra

was done using OMNIC 9.4 software.

### 2.6. Diffusion measurements by infrared spectroscopy

DRIFTS spectra of each sample were collected at a desorption temperature of 473 K under a vacuum pressure of  $10^{-5}$  mbar. Relevant spectral envelope of DBT spectrum (ca.  $1500\text{ cm}^{-1}$  to  $1350\text{ cm}^{-1}$ ) was integrated over the Y zeolite overtone bands (ca.  $2100\text{ cm}^{-1}$ – $1750\text{ cm}^{-1}$ ) were monitored by taking a series of scans. The spectra were collected using the same method described in Section 2.5. To determine the diffusion coefficient, the slope of the desorption curve within the first minute was measured and substituted into the following equation [37]:

$$D_{ns} = \frac{\pi}{36} r^2 (\text{slope})^2 \quad (1)$$

where  $D_{ns}$  is the nonsteady state diffusion coefficient and  $r$  is the particle radius. The initial slope represents the linear relationship between the rate of desorption and the square root of time, enabling the comparison of diffusion length and mass transfer between samples [37,67]. While  $D_{ns}$  may yield a qualitative perspective of the diffusivity of DBT, the values are likely to be perturbed by the presence of physisorbed molecules in the nearby vicinity. In order to exclusively account for chemisorbed DBT, the values must be corrected by a factor of  $C_T/C_0$ :

$$D_{ss} = \frac{C_T}{C_0} D_{ns} \quad (2)$$

where  $D_{ss}$  is the steady state diffusion coefficient,  $C_T$  is the concentration of adsorbed DBT in the zeolite, and  $C_0$  is the initial concentration of DBT introduced into the DRIFTS cell.  $C_T$  can be obtained from calibration curves measured over each zeolite. The calibration curves were derived from the integration of DBT desorption bands over the same Y zeolite overtone bands.

## 3. Results

### 3.1. Characterization results

TEM images of the parent Y, SAY and CeCuY were taken at low magnification to prevent the destruction of samples by the electron beam. The images were captured at the edges of these zeolites to avoid any amorphous region that may arise from the material modification procedure, as well as to elucidate the quality of crystal structures. Fig. 2 shows the structural properties of the parent Y at the nanoscale level. Micropores, as small as 1 nm, were observed (Fig. 2(b)). Fig. 2(c) highlights the diffraction pattern of the sample, confirming the crystalline nature of the parent Y. TEM images of the modified Y zeolites are shown in Fig. 3. Fig. 3(a) shows that the mesoporous Y zeolite contains pores around ~4 nm, which is close to the size of the CTAB micelle [59]. In Fig. 3(b), Scanning Transmission Electron Microscopy (STEM) equipped with elemental mapping highlights Cu and Ce in the CeCuY zeolite. The size of the unreduced metal nanoparticles is relatively small (~2–3 nm) compared to the size of a zeolite particle (~500 nm) and they are well-dispersed in the zeolite extra-framework. Notice that each metal occupies distinct sites in the zeolite.

The physicochemical properties of the materials characterized by  $N_2$  adsorption/desorption are summarized in Table 1. As previously shown, the presence of foreign entities, such as Ce and Cu cations, slightly reduced the surface areas and the microporosity of the parent Y [55]. The introduction of mesopores (eg. SAY, CeSAY, CuSAY, CuCeSAY) reduce the microporosity, while increasing the mesopore surface area and volume of the parent Y. While this is expected, crystallinity of all materials are still comparable as suggested by our previous studies [55]. The SAY zeolites displayed an increase in surface area and pore volume with pores ranging between 20–50 Å.

The chemical composition of the metal-exchanged materials

determined by ICP-MS are also summarized in Table 1. The ICP results show that the metal content in each metal-modified material is within the theoretical value of 5 wt% of metal loading, validating the ion-exchange procedure.

The TPR profile of metal-exchanged and mesoporous metal-exchanged Y zeolites are shown in Fig. S1 in the Supporting information Section. Prior to exposure to  $H_2$ , the materials were first calcined *in-situ* under  $N_2$  at 500 °C for 1 h and allowed to cool to 50 °C. Fig. S1 shows the TPR profile of metal-exchanged Y zeolites. The reduction peak that appears just below 200 °C can be attributed to the reduction from  $Cu^{2+}$  to  $Cu^+$  [68]. The TPR profile of CeY exhibits a broad peak at ca. 600 °C, which indicates a reduction from  $Ce^{4+}$  to  $Ce^{3+}$ , consistent with that reported in the literature [69,70]. While the peaks are not as obvious when plotted on the same scale as CuY, a proper rescale of the peak around 600 °C shows the reduction peak of Ce cations as indicated in the inset. The low intensity of Ce reduction peak could be due to the location of Ce cations on the internal sites of zeolite that require higher  $H_2$  pressure to reduce. Nonetheless, the presence of Ce cations has been verified by ICP following a strong digestion procedure to leach the cations out of the sodalite cages. The incorporation of both metal cations into the Y zeolite results in a reduction peak similar to that of CuY. The TPR profile of CuCeY also shows a slight shift of reduction peak to higher temperature, displaying the influence of Ce on the dispersion and reduction behavior of Cu cations.

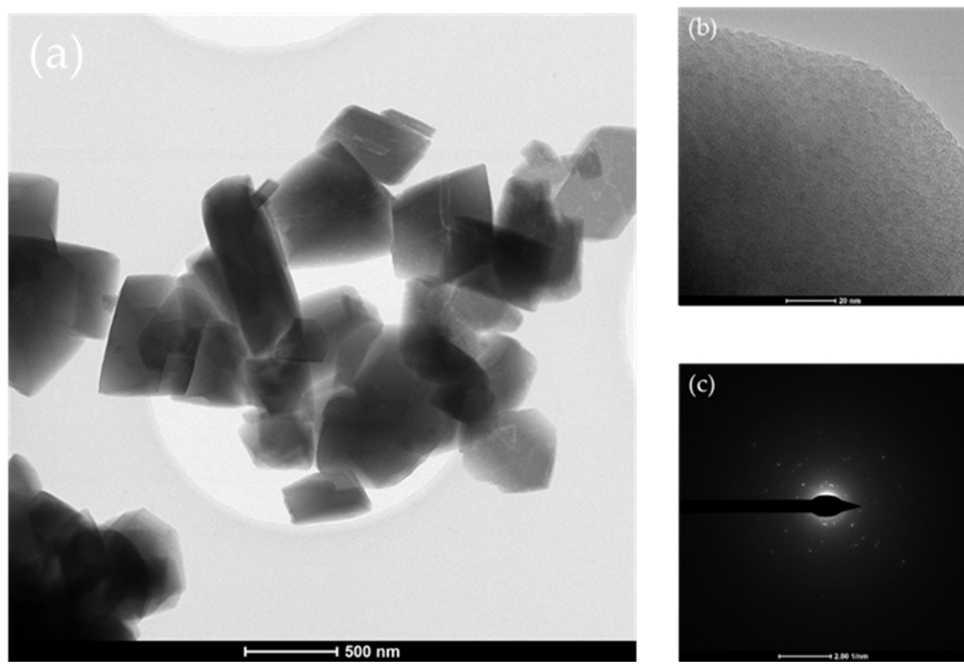
### 3.2. Fixed-bed adsorption results

Fig. 4 shows the breakthrough curves of BT and DBT in a mixture of 80% *n*-octane and 20% benzene on parent and modified Y zeolites. Fig. 4(a) shows that BT breaks through very early on parent Y and reaches saturation within 5 mL/g of feed. When Ce cations were incorporated in the Y zeolite, the breakthrough point was extended from 0.5 mL/g to 8.5 mL/g indicating an increase in the adsorption of BT. CuY showed an even higher adsorption capacity of about 12 mL/g, before traces of BT compounds were detected. An interesting observation is the different slope of the breakthrough curves, resulting from the different kinetics of BT adsorption on the CeY and CuY. This might be attributed to the different configurations of BT adsorption on the two metals. When both Ce and Cu cations were used in the Y zeolite, the ability to adsorb BT increased even more to 15 mL/g of sulfur-free fuel.

The adsorptive desulfurization of DBT in the presence of benzene is presented in Fig. 4(b). Similar to BT, the adsorption capacity of the parent Y is very poor. Previous studies have shown that the poor performance of Y to remove refractory sulfur compounds, such as DBT and 4,6-DMDBT, can be attributed to diffusion limitations [41,55,71,66]. To overcome the aforementioned challenges, SAY was used as a sorbent. It successfully produced at least twice the amount of DBT-free effluent compared to parent Y. The addition of Ce cations to the mesoporous SAY (CeSAY) did not improve the desulfurization performance, most likely due to the allocation of Ce cations on sites that are inaccessible for DBT to enter. CuSAY, on the other hand, showed encouraging improvement in the adsorption capacity of DBT, as the addition of Cu cations extended the breakthrough point from 10 mL/g to 20 mL/g. The enhanced performance of bimetal Y on BT removal, along with the positive results of metal-exchanged mesoporous Y, motivated the use of bimetal-exchanged mesoporous Y (CuCeSAY) for the DBT removal. As observed in Fig. 4(b), CuCeSAY dramatically increases the adsorption capacity of DBT to more than 30 mL/g of clean fuel.

Although significant amount of BT exists in the gasoline range fuels, some BT and especially all DBT is found in the diesel. Diesel also contains aromatics such as naphthalenes and alkyl-naphthalenes. To understand the effect of the simultaneous presence of heavier aromatics on the adsorption of BT and DBT, we performed adsorption experiments using model fuels containing 1 wt% naphthalene and 1 wt %1-methyl-naphthalene in *n*-octane.

Fig. 5 shows the adsorption results of BT and DBT in the model fuel



**Fig. 2.** Low-magnification TEM images of Y zeolite (a) nanoparticles, (b) micropores and (c) diffraction pattern.

containing 1% naphthalene in *n*-octane. As expected, the parent Y zeolite exhibits the lowest BT and DBT capacities and the presence of naphthalene only exacerbates the relatively poor sulfur uptake. For the desulfurization of BT, both metal-exchanged zeolites show slightly higher adsorption capacity, with CeY producing up to 1.5 mL/g of BT-free fuel, while CuY about 2.5 mL/g. This trend is similar to that observed in the removal of BT in 20% benzene. By combining both Ce and Cu, the breakthrough is extended to 5 mL/g of BT-free fuel, confirming that the synergy between the two metals leads to stronger adsorption of sulfur. Fig. 5(b) displays the effect of naphthalene on the desulfurization of DBT. Both SAY and CeSAY displays slightly higher DBT capacity compared to parent Y. The presence of Ce did not improve the desulfurization performance. This phenomenon can be attributed to the limited accessibility of the metal, which has been discussed previously. CuSAY, on the other hand, drives the adsorption capacity to 20 mL/g of clean fuel, which is higher than the capacity observed by CeSAY and SAY. The best sorbent is still, by far, CuCeSAY with a DBT adsorption capacity of about 45 mL/g. This suggest that the synergistic interaction between Ce and Cu plays an important role on the adsorption of refractory sulfur compounds, while the mesoporosity yields higher bulk mass transfer to the internal active sites. While naphthalene is

predominant in diesel and jet fuels, other aromatic hydrocarbons are also present, and can affect the selective adsorption of BT and DBT. Fig. 6 shows the effect of another aromatic compound (1-methyl-naphthalene) on BT and DBT removal. Both Fig. 6(a) and (b) show that the breakthrough may occur earlier. This result could be due to steric hindrance imposed by the methyl group on naphthalene. Nonetheless, results still indicate that CuCeSAY can still maintain a relatively high sulfur capacity, despite the presence of competing aromatics with similar structure.

### 3.3. In situ DRIFTS studies

The adsorption mechanism of sulfur compounds from liquid fuels highly depends on the type of metals in the zeolite and their interaction. To understand the mechanism of BT and DBT adsorption on (bi)metallic zeolites, we performed in-situ DRIFTS experiments in a temperature and atmosphere controlled reaction chamber. Fig. 7 shows the DRIFT spectra of BT on (I) CuY, (II) CeY and (III) CuCeY zeolites recorded from TPD under vacuum in the (a) zeolite region and in the (b) C=C region. Vibrational bands ranging from  $3500\text{ cm}^{-1}$  to  $3750\text{ cm}^{-1}$  are characteristic of the zeolite hydroxyl region. The peak at  $3743\text{ cm}^{-1}$  is

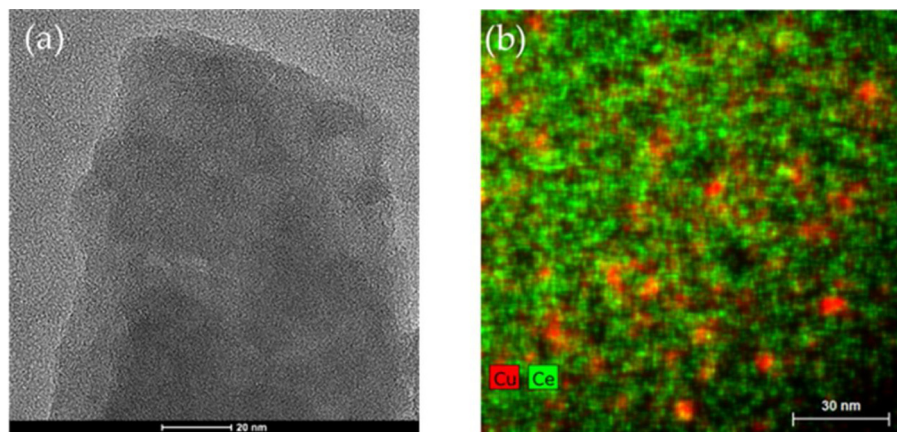


**Fig. 3.** (a) Low-magnification TEM image of mesoporous (SAY) zeolite and (b) STEM image of bimetallic (CeCuY) zeolite.

**Table 1**  
Physical and Chemical Properties of parent and modified Y zeolites.

Material	$S_{tot}$ (m <sup>2</sup> /g)	$S_{micro}$ (m <sup>2</sup> /g)	$S_{meso}$ (m <sup>2</sup> /g)	$V_{tot}$ (cm <sup>3</sup> /g)	$V_{micro}$ (cm <sup>3</sup> /g)	$V_{meso}$ (cm <sup>3</sup> /g)	$Ce^a$ (wt%)	$Cu^a$ (wt%)
Parent Y	574	530	43.9	0.282	0.246	0.036	—	—
CeY	550	500	50.1	0.273	0.232	0.041	5.5	—
CuY	528	475	52.8	0.281	0.229	0.052	—	4.9
CuCeY	549	492	57.2	0.284	0.221	0.063	2.5	2.7
SAY	692	426	319	0.373	0.192	0.201	—	—
CeSAY	648	413	235	0.342	0.190	0.152	5.6	—
CuSAY	637	411	226	0.336	0.190	0.146	—	4.6
CuCeSAY	646	419	227	0.362	0.198	0.164	3.1	2.7

<sup>a</sup> Ce and Cu metal contents were determined using ICP-MS.

attributed to terminal SiOH, while the bands at 3545 cm<sup>-1</sup> and 3635 cm<sup>-1</sup> are attributed to hydroxyl groups in the zeolite framework [59,72]. Any peaks observed above 3000 cm<sup>-1</sup>, are attributed to vibrational stretches of C-H bond of the aromatic rings. Peaks ranging from 1600 cm<sup>-1</sup> to 1300 cm<sup>-1</sup> are mostly due to vibrational stretches of C=C bond of the aromatic rings.

### 3.3.1. Benzothiophene adsorption on CuY

Fig. 7(a)(I) and (b)(I) show the adsorption of BT on CuY. It appears that the acidic hydroxyl sites (ca. 3545 cm<sup>-1</sup> and 3636 cm<sup>-1</sup>) of CuY are occupied rapidly upon exposure to BT vapor. Difference spectra (Fig. S4) also show a change in the intensity of the 3743 cm<sup>-1</sup> band, indicating that the external silanol groups are also participating in the BT adsorption. However, sulfur compounds exhibit higher affinity to adsorb onto the Brønsted acid sites compared to the silanol. As BT vapor began to saturate the zeolite adsorption sites, new peaks start to appear. The band located at 3080 cm<sup>-1</sup> is due to C-H stretching, which confirms the adsorption of BT. By subjecting the sample to TPD, the physisorbed BT vapor is removed from the cell, and the chemisorbed BT can be studied more closely. The adsorption of BT on CuY triggers vibrational stretches and bending of C=C bonds that consequently show up in regions below 1700 cm<sup>-1</sup>, as seen in Fig. 7(b)(I). As CuY undergoes thermal desorption, vibrational bands at 1425 cm<sup>-1</sup>, 1450 cm<sup>-1</sup>, 1585 cm<sup>-1</sup> and 1635 cm<sup>-1</sup> are observed. To understand the significance of these bands, they can be compared to vibrational bands of free BT and of BT-adsorbed on CuO (Figs. S2(a) and S6(a), respectively). In the high wavenumber region, free BT exhibits a peak at 3080 cm<sup>-1</sup>, which is due to C-H vibration, while the peak at 1460 cm<sup>-1</sup> corresponds to symmetrical C=C vibrations. Upon adsorption of BT on the zeolite surface, a shift in the frequency of vibration is expected due to the change in electron density [73,74]. Thus, the peak due to free BT may be shifted to higher or lower wavenumbers (blue shift or red shift, respectively). A red shift in wavenumber suggests a decrease in vibration frequency due to a reduction in electron

density of the adsorbing species. This occurs when an aromatic ring stacks above an active site via  $\pi$ -complexation, in which the metal cation backdonates electron density to the anti-bonding  $\pi$ -orbital of the sulfur ring [75]. Based on the present BT desorption spectra, it can be suggested that the peak at 1425 cm<sup>-1</sup> is attributed to the symmetrical C=C stretching vibration of free BT, which has been shifted to a lower wavenumber. The red shift of the C=C stretching peak suggests an elongation/deformation of the ring due to a reduction in electron density, which can occur when BT ring is adsorbed on Cu via  $\pi$ -complexation. A schematic showing the  $\pi$ -stacking configuration is illustrated in Fig. S10(a). A blank experiment of BT adsorption on parent Y can be also found in Fig. S3.

### 3.3.2. Benzothiophene adsorption on CeY

Fig. 7a(II) and b(II) show the IR spectra of BT adsorption on CeY. It appears that BT adsorption on CeY exhibits the same IR bands generated on CuY, with the addition of an extra peak at 1490 cm<sup>-1</sup>. This peak is attributed to C=C bonds. The appearance of this peak at higher wavenumber relative to free BT (1460 cm<sup>-1</sup>) can be ascribed to an increase in electron density of the BT ring, implying that the adsorption of BT on Ce occurs via direct  $\sigma$ -bond interaction, in addition to  $\pi$ -complexation. [76]. A schematic displaying the direct S-M interaction through  $\sigma$ -bonding is illustrated in Fig. S10(b). These results suggest that Ce can adsorb aromatic sulfur compounds via two types of adsorption modes, which makes it highly beneficial in selective adsorption of sulfur in a mixture of aromatics. This phenomenon was also observed by other rare earth metals or lanthanides-exchanged zeolites [75,77]. One interesting observation is the existence of a shoulder peak near the hydroxyl region at 3515 cm<sup>-1</sup>, which can be viewed more clearly when the spectra are subtracted from the fresh zeolite spectrum, as shown in Fig. S4. This shoulder peak could be attributed to the interaction of Ce cation on the type I' site and the zeolite framework, which could lead to perturbation in the hydroxyl vibrational frequency [78]. This scenario is absent from the CuY zeolite, since Cu cations are mostly populated in

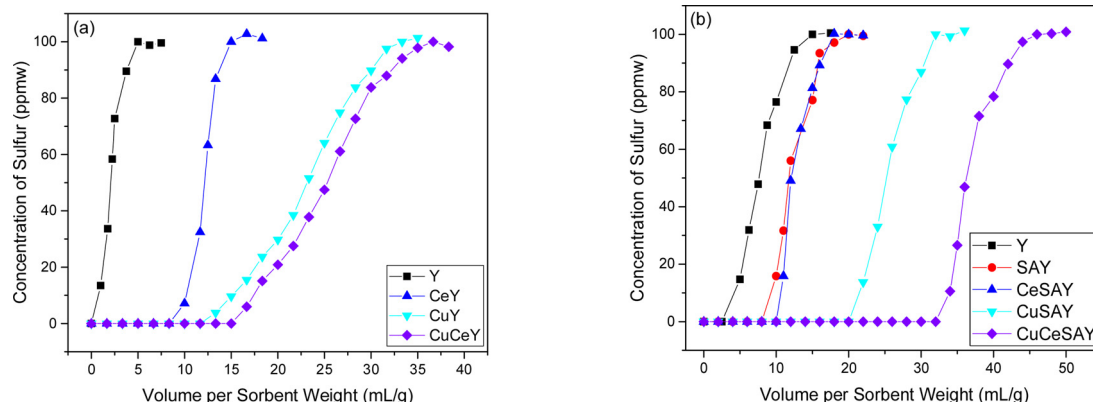


Fig. 4. Breakthrough curves of (a) BT and (b) DBT in a mixture of 80% n-octane and 20% benzene on various Y zeolite adsorbents.

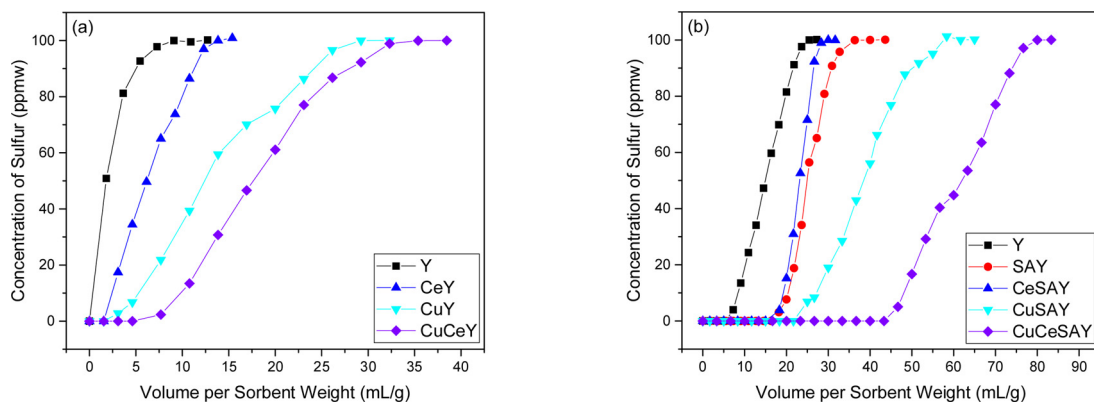


Fig. 5. Breakthrough curves of (a) BT and (b) DBT in a mixture of 99% *n*-octane and 1% naphthalene on various Y zeolite adsorbents.

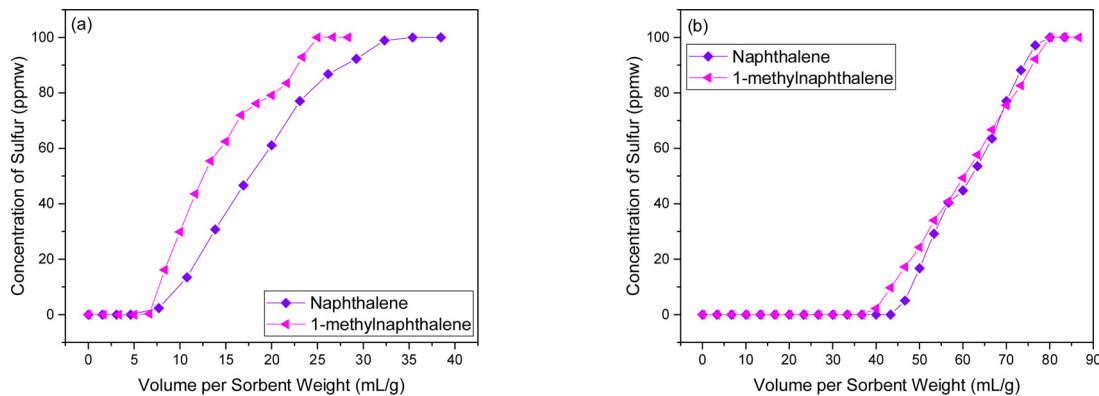


Fig. 6. Breakthrough curves of (a) BT and (b) DBT adsorbed over CuCeY and CuCeSAY, respectively in a mixture of 99% *n*-octane and 1% naphthalene or 1% 1-methylnaphthalene.

the supercage.

### 3.3.3. Benzothiophene adsorption on CuCeY

Fig. 7a(III) and b(III) show the IR spectra of BT adsorption on CuCeY. The peaks are similar to the ones observed with CuY and CeY. These include vibrational bands at  $1425\text{ cm}^{-1}$  and  $1490\text{ cm}^{-1}$  which resulted from  $\pi$ -complexation and  $\sigma$ -bond interaction of BT and CeCuY zeolite. Interestingly, in the case of CuCeY, the  $3635\text{ cm}^{-1}$  vibrational band is not recovered even at high desorption temperatures ( $500\text{ }^\circ\text{C}$ ). This observation suggests that higher temperatures are required to completely desorb BT from the surface, which suggests a stronger interaction between CuCeY and BT compared to the interaction of BT with CuY and CeY. This is also true in the C=C region, where the C=C bond stretching is still apparent even at  $500\text{ }^\circ\text{C}$ . Fig. S4(C) displays the difference spectra of adsorbed BT on CuCeY. The results indicate strong interaction between the sorbent and the sorbate. Another interesting observation is the presence of bands below  $3000\text{ cm}^{-1}$  on CeY and CuCeY, but not on CuY. These bands are usually characteristic of sp<sup>3</sup>-hybridized C–H bonds, which could be due to the elongation of BT ring. This type of interaction can only occur when there is a direct  $\sigma$  interaction as displayed by Ce and CuCeY.

To understand the selectivity of the (bi)metallic zeolites for benzothiophene adsorption, we performed similar *in situ* IR studies as above, using only benzene. The IR spectra of free benzene, as well as the TPD profiles of adsorbed benzene on CuY, CeY and CuCeY are shown in Fig. S8. Free, isolated benzene, shown in Fig. S8(a) shows a strong distinct band at  $3060\text{ cm}^{-1}$  due to C–H vibration of the ring, as well as, a number of C=C vibration bands below  $2000\text{ cm}^{-1}$ . The higher region of the spectrum in Fig. S8(b) shows that the silanol (ca.  $3743\text{ cm}^{-1}$ ) and hydroxyl sites (ca.  $3635\text{ cm}^{-1}$  and  $3545\text{ cm}^{-1}$ ) are the preferred sites for benzene adsorption. The presence of benzene, both physisorbed and

chemisorbed, is evidenced by the C–H band at  $3040\text{ cm}^{-1}$  and  $3060\text{ cm}^{-1}$ , respectively. Upon evacuation, most of benzene has been desorbed by  $100\text{ }^\circ\text{C}$ . In the C=C vibration region (Fig. S8(c)), all three zeolites exhibit a band at  $1475\text{ cm}^{-1}$ . This band represents a red shift of the C=C vibrational band from  $1490\text{ cm}^{-1}$  to lower wavenumber ( $1475\text{ cm}^{-1}$ ) and can be attributed to the interaction of benzene ring with the CuY, CeY and CuCeY through  $\pi$ -complexation. This result confirms that CeY and CuCeY are more selective for BT via additional adsorption configurations ( $\sigma$ -bonding).

### 3.3.4. Dibenzothiophene adsorption

Fig. 8 displays the corresponding IR results of DBT adsorption on metal-exchanged mesoporous SAY. Mesoporous SAY zeolites were used for the adsorption of DBT to overcome diffusion limitations. Free DBT exhibits peaks attributed to the symmetrical C=C vibration bonds at  $1450\text{ cm}^{-1}$ , as shown in Fig. S2(b) [79]. Similar to BT, the acidic hydroxyl sites (ca.  $3635\text{ cm}^{-1}$  and  $3550\text{ cm}^{-1}$ ) were rapidly covered with physisorbed DBT compounds, as seen in Fig. 8(a). This confirms that the Brønsted acid sites form stronger complexes with the studied sulfur molecules, while the external silanols hardly contribute to the adsorption. In fact, only the hydroxyl site in the supercage (ca.  $3635\text{ cm}^{-1}$ ) is responsible for the adsorption of DBT. This phenomenon is consistent with our previous finding that Cu cations are located in type II sites located in the supercage [55]. Furthermore, the bulky nature of DBT could prevent further interaction with Brønsted sites in the sodalite cages. Fig. 8(b)(I) shows that CuSAY exhibits three bands located at  $1422\text{ cm}^{-1}$ ,  $1445\text{ cm}^{-1}$  and  $1590\text{ cm}^{-1}$ . The bands at  $1422\text{ cm}^{-1}$  and  $1445\text{ cm}^{-1}$  are a consequence of a red shift from  $1450\text{ cm}^{-1}$  of free DBT, implying a loss of electron density. Thus, similar to the adsorption of BT, DBT adsorbs on CuSAY via  $\pi$  stacking. When DBT was adsorbed onto CeSAY, an additional peak was observed in the O–H region

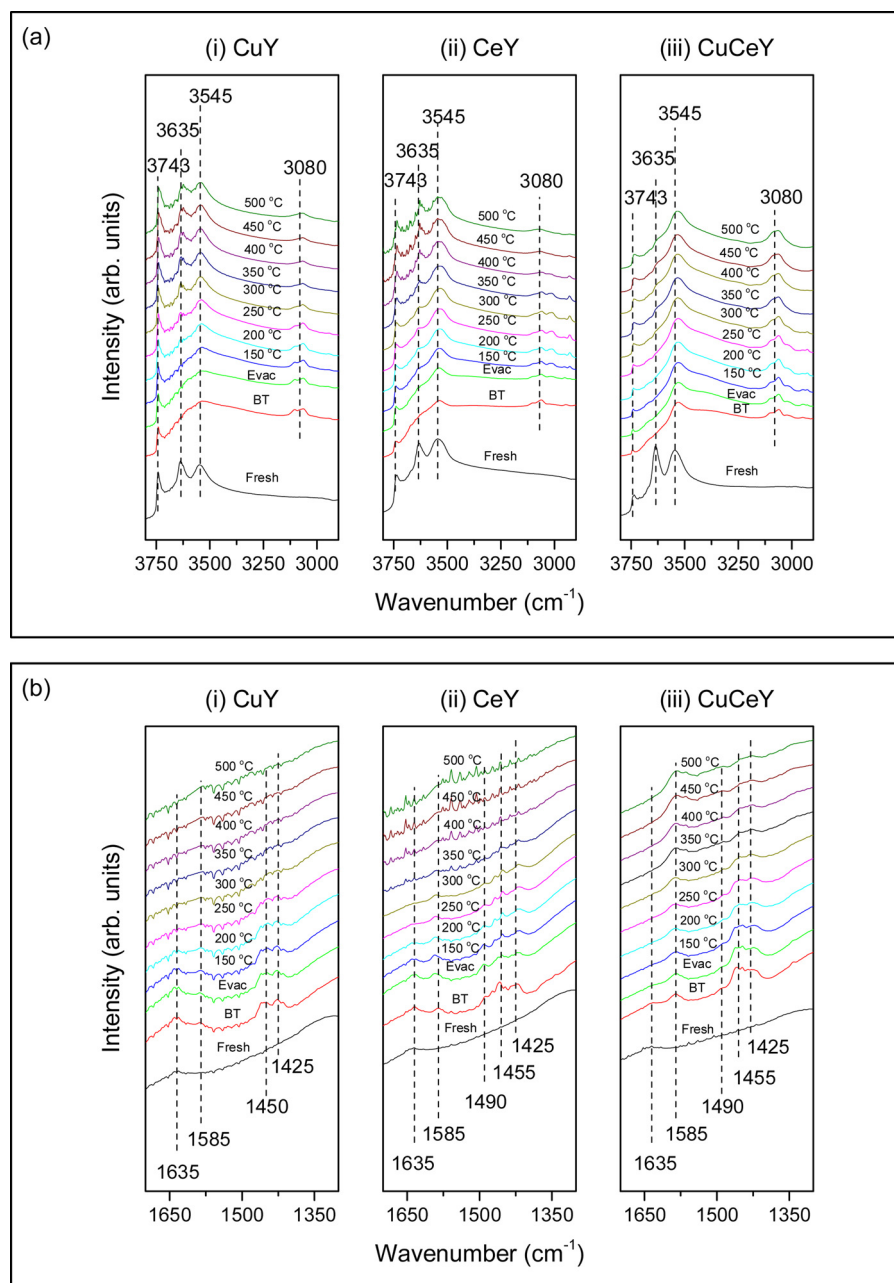


**Fig. 7.** FTIR spectra during BT adsorption and temperature-programmed desorption on (i) CuY, (ii) CeY and (iii) CuCeY of the (a) zeolitic region and the (b) C=C region of the sulfur molecule.

(Fig. 8(b)(II)). The peak can be seen more clearly in Fig. S5(b). The peak at 3500 cm<sup>-1</sup> could be attributed to Ce cation interaction with the hydroxyl sites located in the sodalite cages, similar to the peak at 3515 cm<sup>-1</sup> on CeSAY. In the C=C region, an additional peak appeared along with those observed on CuSAY. Upon adsorption, the peak of free DBT at 1450 cm<sup>-1</sup> has been positively shifted by 10 cm<sup>-1</sup> to 1460 cm<sup>-1</sup>. The blue shift of this peak suggests that a direct interaction between the Ce cation of CeSAY and the sulfur atom of DBT ring has occurred. The adsorption of DBT on CeSAY via the σ-bond or  $\eta^{1s}$  configuration has also been observed theoretically [80]. To confirm that the peak at 1460 cm<sup>-1</sup> is due to σ-bond interaction, the adsorption of DBT was also studied over CeO<sub>2</sub>. The spectrum (Fig. S7(b)) displays an additional peak at 1460 cm<sup>-1</sup>, confirming the direct S–M interaction due to Ce. To confirm that the bands are in fact indicative of the suggested mechanisms, DBT was also allowed to adsorb on CuCeSAY (Fig. 8(a)(III) and (b)(III)). The result shows that the bimetallic

mesoporous zeolite exhibits the same characteristic bands as those on CeSAY, which confirms the ability to form π-complexation and σ-bond interaction. The presence of Ce cations can also be inferred by the appearance of the shoulder at 3500 cm<sup>-1</sup>. Similar to BT adsorption on CuCeY, a relatively higher temperature is required to completely desorb DBT from CuCeSAY, due to the strong synergetic effect of Cu and Ce. The use of CuCeSAY as a sorbent material not only allows refractory sulfur compounds to access the active sites via its mesopores, but the presence of Ce and Cu cations play a crucial role in the adsorption of sulfur molecule.

Additionally, the selectivity of CeCuSAY for DBT can be examined by comparing and studying the adsorption of naphthalene using *in situ* IR studies. Fig. S9 shows the IR spectrum of free naphthalene, as well as the adsorbed and desorbed IR profiles of naphthalene over the ion-exchanged mesoporous zeolites. The figure shows that free naphthalene exhibits clear stretching bands at 3060, 1600, 1510 and 1390 cm<sup>-1</sup>.

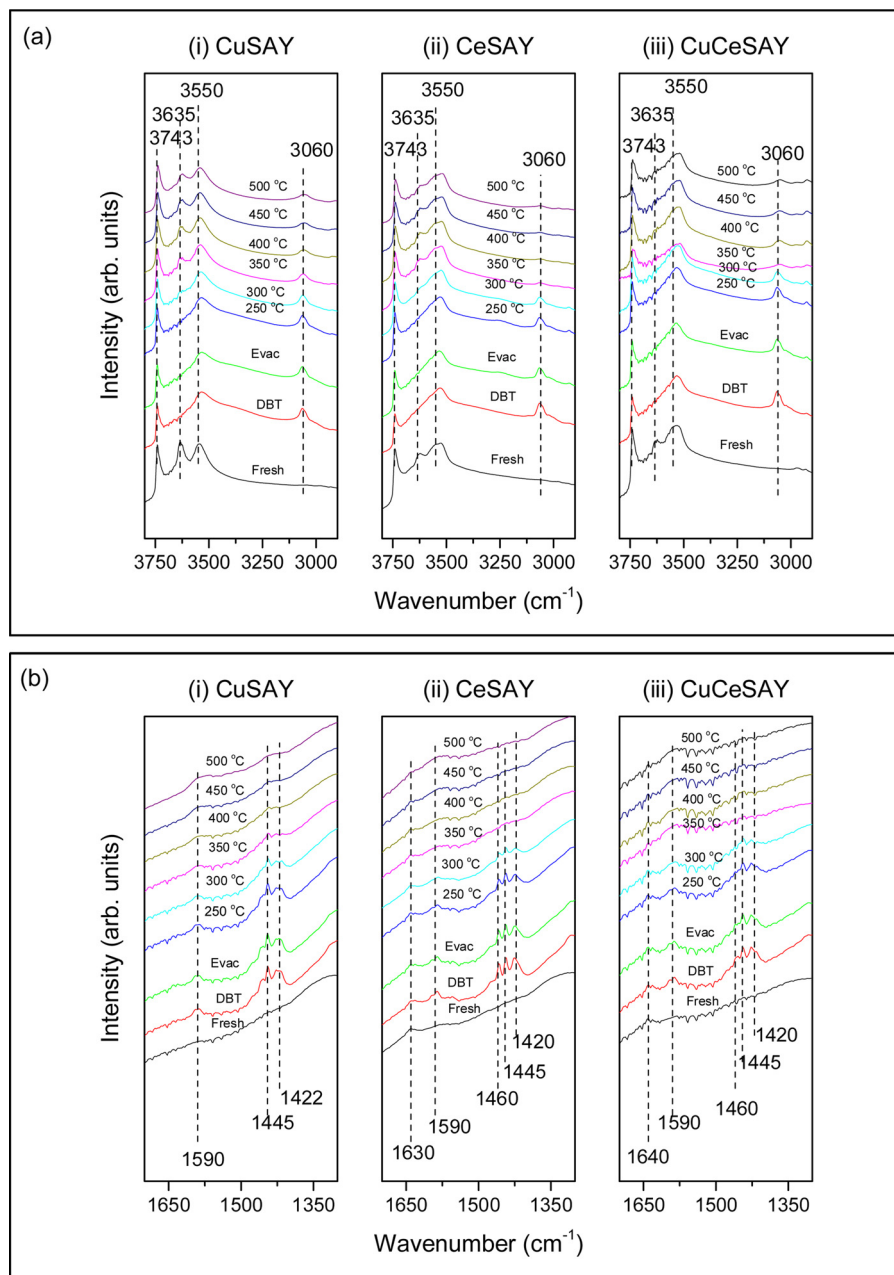


**Fig. 8.** FTIR spectra during DBT adsorption and temperature-programmed desorption on (i) CuSAY, (ii) CeSAY and (iii) CeCeSAY of the (a) zeolithic region and the (b) C=C region of the sulfur molecule.

The first band at 3060 cm<sup>-1</sup> is due to stretching of C–H bonds, while the other three bands correspond to both symmetrical and asymmetrical bending of the C=C bonds. Fig. S9(b) clearly shows that the preferred adsorption sites of naphthalene are the hydroxyl sites located at 3635 cm<sup>-1</sup> and 3550 cm<sup>-1</sup>. The presence of chemisorbed naphthalene can be confirmed by the C=C characteristic band at 3060 cm<sup>-1</sup>, consistent to that of free naphthalene. When subjected to TPD, the covered hydroxyl sites begin to reappear at higher temperature, suggesting desorption of naphthalene. By 500 °C, almost all of the active sites have been restored and most of the naphthalene has been desorbed. Fig. S9(c) shows the C=C vibration region of naphthalene upon adsorption on the mesoporous zeolites. The predominant vibration bands are located at 1590, 1500 and 1390 cm<sup>-1</sup>, most of which resulted from a negative shift to lower wavenumbers. This indicates that the adsorption of naphthalene only undergoes  $\pi$ -complexation, similar to the adsorption of benzene. In comparison to the adsorption of DBT, TPD

profiles indicate that a higher temperature is required to completely desorb DBT, due to strong interaction from both  $\pi$ -complexation and  $\sigma$ -bonding. Subsequently, DBT displays higher heat of adsorption compared to naphthalene [81]. The corroboration of additional adsorption bands and higher binding energy altogether supports the conclusion that CeCeSAY is more selective for DBT compared to competing aromatics, such as naphthalene.

### 3.4. Mass transfer studies of mesoporous Y zeolite

To investigate the mass transfer limitations of DBT adsorption in Y zeolite, we conducted desorption experiments *via in situ* DRIFTS. The bands due to desorption of DBT (ca. from 1350 cm<sup>-1</sup> to 1500 cm<sup>-1</sup>) were integrated over the zeolite overtone band (ca. from 2100 cm<sup>-1</sup> to 1750 cm<sup>-1</sup>) in real time and were plotted against the square root of time, as shown in Fig. 9. DBT desorbs more rapidly on SAY compared to

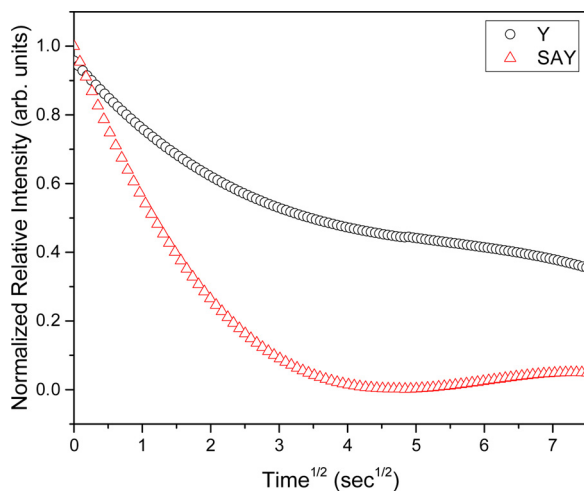


**Fig. 9.** Desorption of DBT at 473 K from Y and mesoporous Y (SAY) under  $10^{-5}$  mbar.

**Table 2**

Nonsteady state ( $D_{ns}$ ) and steady state ( $D_{ss}$ ) diffusion coefficients of DBT on Y and mesoporous Y (SAY).

Zeolite	$D_{ns}$ (cm <sup>2</sup> /s)	$D_{ss}$ (cm <sup>2</sup> /s)
Y	$2.09 \times 10^{-14}$	$1.51 \times 10^{-14}$
SAY	$1.05 \times 10^{-13}$	$6.72 \times 10^{-14}$

Y, as indicated by the steepness of the desorption curves. This behavior can be attributed to the available mesopores in SAY, which allow DBT, a relatively large sulfur compound, to diffuse more rapidly towards the internal active sites. For qualitative comparison, the slope of each curve was taken to calculate the nonsteady state and ultimately, the steady state diffusion coefficients of DBT on each zeolite, as depicted in **Table 2**. Due to the incorporation of mesopores, SAY exhibits 4.5x the diffusivity compared to the microporous Y. This result confirms that hierarchical pore zeolites can reduce diffusion limitation, and thus effectively increasing the sulfur adsorption capacity, as shown by the breakthrough curves in **Figs. 4–6**.

#### 4. Discussion

In our previous work we studied the adsorptive desulfurization of BT and DBT on Cu, Ce and CuCeY zeolites using n-octane as a model fuel [55]. Motivated by the encouraging results of that work, here, we investigate the adsorptive desulfurization of BT and DBT in the presence of aromatic hydrocarbons. Our previous work showed that metal-exchanged Y zeolite exhibits high sulfur adsorption capacity in n-octane. This present study has focused on: a) the effect of aromatics on the adsorptive desulfurization of sulfur compounds from fuels, and b) the mechanism of adsorption of sulfur compounds on Y zeolites. Benzene, naphthalene and methyl-naphthalene were used as the competing aromatic molecules. Benzene is an aromatic molecule found in the gasoline range fuel, but it was used in this study as the primary model molecule, due to the simplicity of its structure. Naphthalene and methyl-naphthalene were also used as model aromatics, because they are abundant in jet and diesel range fuels.

The breakthrough curves in **Fig. 4** reveal that the sulfur compounds show up much earlier when benzene is present in the fuel, compared to the aromatic-free sulfur fuel [55]. The addition of benzene resulted in a decrease in breakthrough volume of about 5 mL/g on the parent Y. According to the literature, Y zeolites can adsorb aromatic compounds via  $\pi$ -complexation and/or direct H–bonding, but these interactions are relative weak and unselective [82]. As a result, the parent Y can adsorb

benzene and thus, compromising the selective adsorption of thiophenic compounds. Without benzene in the feed, CeY and CuY both reported very high adsorption capacities for BT, where 35 mL/g and 65 mL/g of clean fuel were produced, respectively [55]. However, in the presence of benzene, the same sorbents were not able to meet the same results; thus, less than 15 mL/g of BT-free fuel was produced. The highest capacity of BT in the presence of benzene, however, was displayed by CuCeY, which resulted to 15 mL/g of BT-free fuel. One interesting observation about these results is that the breakthrough curves show different adsorption slopes. A steep slope was seen on parent Y and CeY, whereas a gradual increase in sulfur concentration was displayed on CuY and CuCeY. The difference in slope could be attributed to different adsorption kinetics, which are dictated by mass transfer to the active site and/or the type of adsorption configuration [83–85]. Ce cations have been shown to preferentially disperse within the sodalite cage, which is too small for thiophenic compounds to enter. The limited amount of accessible Ce sites cause the sorbent to be saturated more rapidly. Moreover, Ce cations have shown to favor strong  $\sigma$ -bond formation by donating a 4f electron to sulfur, which could also increase the adsorption kinetics [86]. These characteristics of Ce result in fast adsorption rate, leading to a steeper slope compared to Cu.

Similar trends were also observed on the removal of DBT. On parent Y, DBT broke through as early as 3 mL/g of liquid feed, which is about 15 times faster than it was compared to the desulfurization of the same compound without benzene [55]. Note that the elution time of DBT was longer relative to that of BT. In our previous work, we have shown that electron density increases with the size of sulfur compound, which explains the tendency to adsorb of DBT to adsorb more strongly than BT on the parent Y [55]. The same trend is also observed on metal-exchanged and SAY zeolites, confirming the preferential order to adsorb the aforementioned sulfur compounds. SAY showed higher adsorption capacity of DBT, producing 8 mL/g of sulfur free liquid fuel in the presence of benzene. In the presence of naphthalene and 1-methyl-naphthalene, CuCeSAY produced up to 45 mL/g and 40 mL/g of DBT-free fuel. As expected, the removal of DBT is mass transfer limited due to the large kinetic diameter, and thus the introduction of mesopores allowed the larger molecule to access the internal active sites of the micropores. The effect of mesoporosity on the adsorption of DBT was also observed in our in-situ IR studies. Results (not shown here) have displayed the lack of vibrational bands on parent Y zeolites, indicating the absence of DBT adsorption. The easier diffusion of DBT in mesoporous Y compared to the corresponding microporous was also confirmed by the diffusion measurements in Section 3.4.

Surprisingly, the breakthrough curve of CeSAY was similar to that of SAY, suggesting little or no improvement of sulfur removal. According to the literature, Ce cations develop high preference to coordinate mainly with type I' sites, which are located in the sodalite cages [87,88]. This may be the reason for the low adsorption capacity of CeSAY, since DBT may be too large to access the sodalite cage. Meanwhile, 20 mL/g of DBT-free fuel was produced by CuSAY, which is twice as much compared to metal-free SAY. This improvement is a result of the relatively strong interaction that Cu metals can form with DBT via  $\pi$ -complexation and the more accessible type II and II' sites which Cu occupies [89,90].

We also performed more modifications to our mesoporous Y material by ion-exchanging mesoporous Y with two metal cations (Ce and Cu) to make CuCeSAY. While limited studies on metal-exchanged mesoporous zeolites for sulfur adsorption have been reported, the role of bimetal mesoporous Y zeolite has yet to be explored [71,91]. Moreover, bimetal-exchanged zeolites have been proven to possess high selectivity and capacity for sulfur compounds [58,76]. The performance of CuCeSAY is demonstrated in **Fig. 4(b)**, which shows a 3-fold increase in sulfur removal capacity compared to the performance of SAY. To the best of our knowledge, this is yet the highest DBT adsorption capacity observed. Yang and co-workers conducted similar fixed-bed adsorption experiment of DBT in 20% benzene and 80% n-octane and showed that

CuY had the highest adsorption capacity by producing 20 mL/g of DBT-free fuel, followed by siliceous MCM-41 and activated carbon (AC) [92]. This confirms our hypothesis that in addition to the enhancement in mass transfer, the synergistic effect of Cu and Ce metals increases the selectivity and capacity for DBT in the presence of benzene. It is important to note that Ce alone does not possess high capacity of sulfur as shown in Figs. 4 and 5 for either BT or DBT. Additionally, the coordination of Ce cations in the sodalite cages do not warrant easy access to these sites. Yet, the presence of Ce seemed to play an important role when used as a secondary metal in CuCeSAY as demonstrated from the breakthrough curve. According to Shan et al. the presence of Ce species in the extra-framework speeds up the auto-reduction of  $\text{Cu}^{2+}$  to  $\text{Cu}^+$  and consequently enhances the density of  $\text{Cu}^+$  cations, which is the optimum oxidation state to adsorb sulfur molecules [60]. The tendency of each metal to occupy different coordination sites in the extra-framework, as suggested by the TEM images in Fig. 3(b), leads to a higher probability that most of the active sites have been ion-exchanged with either Ce or Cu. The resulting bimetal-exchanged mesoporous Y zeolite has shown to exhibit exceptional desulfurization capabilities.

These results have also been confirmed by our desorption studies using *in-situ* DRIFT. As demonstrated in Fig. 7, the synergistic effect of Cu and Ce in zeolite Y leads to a relatively high recovery temperature. Similarly, Fig. 8 shows that it takes a higher temperature to completely desorb DBT from CuCeSAY. It has also been shown that the recovery of the supercage is relatively slower during the desorption of both BT and DBT. This suggests that the interaction between the sulfur compounds and active sites occurs predominantly in the supercage. This also explains the relatively low sulfur capacity of Ce and CeSAY compared to other modified material (Figs. 4 and 5), since Ce is mostly found in the sodalite cages. Although the adsorption of sulfur on Ce is strong and selective, the location and the tendency to form strictly one-to-one  $\sigma$ -bond do not contribute to higher sulfur capacity. Meanwhile, CuY and CuSAY have shown higher adsorption capacity because of the possibility of multilayer adsorption via  $\pi$ -stacking [93]. Nonetheless, the presence of Ce in the inner cages has shown to increase the strength and dispersion of Cu. This is evidenced by both the improved breakthrough results shown by the fixed-bed experiment, as well as the extremely strong sorbent-sorbate interaction shown by the DRIFT analysis. The role of Ce on the electronic properties of Cu for sulfur adsorption will be investigated in our future studies. The adsorption studies of both benzene and naphthalene also shed light on the selectivity of bimetallic CuCeY and CuCeSAY zeolites. It was apparent that benzene and naphthalene desorbed at lower temperature compared to BT and DBT, respectively. Subsequently, the adsorption of the aromatics proceeded via  $\pi$ -complexation only, which makes CuCeY and CuCeSAY more selective for sulfur compounds in the presence of competing aromatics.

## 5. Conclusion

In this study we have explored the effect of aromatics, such as benzene, naphthalene and methyl-naphthalene, on the adsorptive desulfurization of BT and DBT from model fuels. Among the tested Y zeolite sorbents, bimetal-exchanged zeolites, prepared by ion-exchanging Y zeolites with Cu and Ce, have shown to exhibit high capacity for BT. Such improvement is a result of the synergistic interaction between the two metal cations that lead to stronger interaction with BT via  $\pi$ -complexation and/or  $\sigma$ -bonding. Consequently, about 15 mL/g and 5 mL/g more BT-free fuel in the presence of benzene and naphthalene, respectively, were produced using CuCeY, compared to parent Y. During the adsorptive desulfurization of DBT, diffusion limitations and the presence of benzene, naphthalene and methyl-naphthalene, severely affected the high capacity of zeolite. We proposed that bimetallic mesoporous zeolite (CuCeSAY) would overcome these challenges. The experimental results indicated that CuCeSAY exhibits relatively high DBT capacity of about 32 mL/g in the presence of benzene, and 45 mL/g in the presence of naphthalene. The significant removal of DBT

was also attributed to synergistic effects of: a) the mesopores in Y, which provided access for DBT to the metal cations, and b) of Cu and Ce in CuCeSAY, which resulted in stronger interaction and more adsorption configurations. The tendency to adsorb the tested sulfur compounds follow the order of BT < DBT, suggesting that the influence of electron density on adsorptive desulfurization should not be neglected. From this study, the prepared CuCeSAY has shown to exhibit high potential to become a prominent adsorbent material in commercial and industrial applications. Our future goal is to implement this novel and industrially-viable technology toward real gasoline, jet fuel and diesel.

## Acknowledgement

This work was supported by the American Chemical Society (PRF + 55900-DN15).

## Appendix A. Supplementary data

Supplementary material related to this article can be found, in the online version, at doi:<https://doi.org/10.1016/j.apcatb.2018.04.022>.

## References

- [1] C. Song, An overview of new approaches to deep desulfurization for ultra-clean gasoline, diesel fuel and jet fuel, *Catal. Today* 86 (2003) 211–263, [http://dx.doi.org/10.1016/S0920-5861\(03\)00412-7](http://dx.doi.org/10.1016/S0920-5861(03)00412-7).
- [2] U.S. Energy Information Administration, Spot Prices for Crude Oil and Petroleum Products, (2016) . (Accessed 24 May 2017) [http://www.eia.gov/dnav/pet/pet\\_pri\\_spt\\_s1\\_d.htm](http://www.eia.gov/dnav/pet/pet_pri_spt_s1_d.htm).
- [3] B. Rakita, V. Madic, D. Markovic, Competitive strategies of late followers in auto industry: case study Hyundai-Kia, *Industrija* 45 (2017) 121–146, <http://dx.doi.org/10.5937/industrija45-11848>.
- [4] D.P. Gamlief, H.J. Cho, W. Fan, J.A. Valla, On the effectiveness of tailored mesoporous MFI zeolites for biomass catalytic fast pyrolysis, *Appl. Catal. A Gen.* 522 (2016) 109–119, <http://dx.doi.org/10.1016/j.apcata.2016.04.026>.
- [5] D.P. Gamlief, L. Wilcox, J.A. Valla, The Effects of Catalyst Properties on the Conversion of Biomass via Catalytic Fast Hydropyrolysis, (2016), <http://dx.doi.org/10.1021/acs.energyfuels.6b02781>.
- [6] U.S. Environmental Protection Agency, Integrated Science Assessment for Oxides of Nitrogen – Health Criteria, (2016) . (Accessed 21 November 2016) <https://www.epa.gov/isa/integrated-science-assessment-isa-nitrogen-dioxide-health-criteria>.
- [7] U.S. Environmental Protection Agency, Integrated Science Assessment for Sulfur Oxides – Health Criteria, (2009) . (Accessed 21 November 2016) <https://www.epa.gov/isa/integrated-science-assessment-isa-sulfur-dioxide-health-criteria>.
- [8] V.M. Bhandari, C.H. Ko, J.G. Park, S.S. Han, S.H. Cho, J.N. Kim, Desulfurization of diesel using ion-exchanged zeolites, *Chem. Eng. Sci.* 61 (2006) 2599–2608, <http://dx.doi.org/10.1016/j.ces.2005.11.015>.
- [9] J.A. Valla, A.A. Lappas, I.A. Vasalos, C.W. Kuehler, N.J. Gudde, Feed and process effects on the in situ reduction of sulfur in FCC gasoline, *Appl. Catal. A Gen.* 276 (2004) 75–87, <http://dx.doi.org/10.1016/j.apcata.2004.07.042>.
- [10] H.N. Sharma, V. Sharma, A.B. Mhadeshwar, R. Ramprasad, Why Pt survives but Pd suffers from SOx poisoning? *J. Phys. Chem. Lett.* 6 (2015) 1140–1148, <http://dx.doi.org/10.1021/jz5027147>.
- [11] C. Song, X. Ma, New design approaches to ultra-clean diesel fuels by deep desulfurization and deep dearomatization, *Appl. Catal. B Environ.* 41 (2003) 207–238, [http://dx.doi.org/10.1016/S0926-3373\(02\)00212-6](http://dx.doi.org/10.1016/S0926-3373(02)00212-6).
- [12] J.H. Kim, X. Ma, A. Zhou, C. Song, Ultra-deep desulfurization and denitrogenation of diesel fuel by selective adsorption over three different adsorbents: a study on adsorptive selectivity and mechanism, *Catal. Today* 111 (2006) 74–83, <http://dx.doi.org/10.1016/j.cattod.2005.10.017>.
- [13] U.S. Environmental Protection Agency, EPA Sets Tier 3 motor Vehicle Emissions and Fuel Standards, (2014) . (Accessed 2 March 2016) <https://www.epa.gov/regulations-emissions-vehicles-and-engines/final-rule-control-air-pollution-motor-vehicles-tier-3>.
- [14] J.A. Valla, A.A. Lappas, I.A. Vasalos, Catalytic cracking of thiophene and benzothiophene: mechanism and kinetics, *Appl. Catal. A Gen.* 297 (2006) 90–101, <http://dx.doi.org/10.1016/j.apcata.2005.08.049>.
- [15] J.A. Valla, E. Mouriki, A.A. Lappas, I.A. Vasalos, The effect of heavy aromatic sulfur compounds on sulfur in cracked naphtha, *Catal. Today* 127 (2007) 92–98, <http://dx.doi.org/10.1016/j.cattod.2007.05.017>.
- [16] A.A. Lappas, J. Valla, I.A. Vasalos, C.W. Kuehler, J. Francis, P. O'Connor, et al., Sulfur reduction in FCC gasoline: sulfur removal from gasoline and distillate streams, *Prepr. - Am. Chem. Soc. Div. Pet. Chem.* 47 (2002) 50–52.
- [17] H. Wang, S. Liu, R. Govindarajan, K.J. Smith, Preparation of Ni-Mo2C/carbon catalysts and their stability in the HDS of dibenzothiophene, *Appl. Catal. A Gen.* 539 (2017) 114–127, <http://dx.doi.org/10.1016/j.apcata.2017.04.008>.
- [18] F.J. Méndez, O.E. Franco-López, X. Bokhimi, D.A. Solís-Casados, L. Escobar-Alarcón, T.E. Klimova, Dibenzothiophene hydrodesulfurization with NiMo and CoMo catalysts supported on niobium-modified MCM-41, *Appl. Catal. B Environ.*

- 219 (2017) 479–491, <http://dx.doi.org/10.1016/j.apcatb.2017.07.079>.
- [19] A.T. Atimtay, L.D. Gasper-Galvin, J.A. Poston, Novel supported sorbent for hot gas desulfurization, *Environ. Sci. Technol.* 27 (1993) 1295–1303, <http://dx.doi.org/10.1021/es00044a002>.
- [20] A. Bakr, S.H. Salem, Naphtha desulfurization by adsorption, *Ind. Eng. Chem. Res.* 33 (1994) 336–340, <http://dx.doi.org/10.1021/ie00026a025>.
- [21] E.S. Kikkilides, V.I. Sikavitsas, R.T. Yang, Natural-gas desulfurization by adsorption-feasibility and multiplicity of cyclic steady-states, *Ind. Eng. Chem. Res.* 34 (1995) 255–262, <http://dx.doi.org/10.1021/ie00040a027>.
- [22] Y. Yang, H. Lu, P. Ying, Z. Jiang, C. Li, Selective dibenzothiophene adsorption on modified activated carbons, *Carbon N. Y.* 45 (2007) 3042–3044, <http://dx.doi.org/10.1016/j.carbon.2007.10.016>.
- [23] M. Xue, R. Chitrakar, K. Sakane, T. Hirotsu, K. Ooi, Y. Yoshimura, et al., Selective adsorption of thiophene and 1-benzothiophene on metal-ion-exchanged zeolites in organic medium, *J. Colloid Interface Sci.* 285 (2005) 487–492, <http://dx.doi.org/10.1016/j.jcis.2004.12.031>.
- [24] Y. Wang, R.T. Yang, J.M. Heinzel, Desulfurization of jet fuel by  $\pi$ -complexation adsorption with metal halides supported on MCM-41 and SBA-15 mesoporous materials, *Chem. Eng. Sci.* 63 (2008) 356–365, <http://dx.doi.org/10.1016/j.ces.2007.09.002>.
- [25] J.M. Palomino, D.T. Tran, A.R. Karem, C.A. Miller, J.M.V. Gardner, H. Dong, et al., Zirconia-silica based mesoporous desulfurization adsorbents, *J. Power Sources* 278 (2015) 141–148, <http://dx.doi.org/10.1016/j.jpowsour.2014.12.043>.
- [26] A.J. Hernández-Maldonado, F.H. Yang, G. Qi, R.T. Yang, Desulfurization of transportation fuels by  $\pi$ -complexation sorbents: Cu(I), Ni(II), and Zn(II)-zeolites, *Appl. Catal. B Environ.* 56 (2005) 111–126, <http://dx.doi.org/10.1016/j.apcatb.2004.06.023>.
- [27] S. Velu, X. Ma, C. Song, Selective adsorption for removing sulfur from jet fuel over zeolite-based adsorbents, *Ind. Eng. Chem. Res.* 42 (2003) 5293–5304, <http://dx.doi.org/10.1021/ie020995p>.
- [28] K. Li, J. Valla, J. García-Martínez, Realizing the commercial potential of hierarchical zeolites: new opportunities in catalytic cracking, *ChemCatChem* 6 (2014) 46–66, <http://dx.doi.org/10.1002/cetc.201300345>.
- [29] J. Rabo, P.H. Angell, P.H. Kasai, V. Schomaker, *Tudies Cations Zeolites: Adsorption Carbon Monoxide; Formation Ni Ions Na<sub>3</sub>+ 4 Centres* 41 (1966), pp. 328–349.
- [30] J.F. Denayer, W. Souverijns, P.A. Jacobs, J.A. Martens, G.V. Baron, High-temperature low-pressure adsorption of branched C 5–C 8 alkanes on zeolite beta, ZSM-5, ZSM-22, zeolite Y, and mordenite, *J. Phys. Chem. B* 102 (1998) 4588–4597, <http://dx.doi.org/10.1021/jp980674k>.
- [31] H.W. Langmi, A. Walton, M.M. Al-Mamouri, S.R. Johnson, D. Book, J.D. Speight, et al., Hydrogen adsorption in zeolites A, X, Y and RHO, *J. Alloys Compd.* 356–357 (2003) 710–715, [http://dx.doi.org/10.1016/S0925-8388\(03\)00368-2](http://dx.doi.org/10.1016/S0925-8388(03)00368-2).
- [32] P.J.E. Harlick, F.H. Tezel, An experimental adsorbent screening study for CO<sub>2</sub> removal from N2, *Microporous Mesoporous Mater.* 76 (2004) 71–79, <http://dx.doi.org/10.1016/j.micromeso.2004.07.035>.
- [33] N. Roostaei, F.H. Tezel, Removal of phenol from aqueous solutions by adsorption, *J. Environ. Manage.* 70 (2004) 157–164, <http://dx.doi.org/10.1016/j.jenvman.2003.11.004>.
- [34] A.M. Yusof, N.A.N.N. Malek, Removal of Cr(VI) and As(V) from aqueous solutions by HDTMA-modified zeolite Y, *J. Hazard. Mater.* 162 (2009) 1019–1024, <http://dx.doi.org/10.1016/j.jhazmat.2008.05.134>.
- [35] M.S. Holm, E. Taarning, K. Egeblad, C.H. Christensen, Catalysis with hierarchical zeolites, *Catal. Today* 168 (2011) 3–16, <http://dx.doi.org/10.1016/j.cattod.2011.01.007>.
- [36] W. Lutz, Zeolite Y: synthesis, modification, and properties—a case revisited, *Adv. Mater. Sci. Eng.* 2014 (2014), <http://dx.doi.org/10.1155/2014/724248>.
- [37] F.C. Meunier, D. Verboekend, J.P. Gilson, J.C. Groen, J. Pérez-Ramírez, Influence of crystal size and probe molecule on diffusion in hierarchical ZSM-5 zeolites prepared by desilication, *Microporous Mesoporous Mater.* 148 (2012) 115–121, <http://dx.doi.org/10.1016/j.micromeso.2011.08.002>.
- [38] M. Moliner, Direct synthesis of functional zeolitic materials, *ISRN Mater. Sci.* 2012 (2012) 1–24, <http://dx.doi.org/10.5402/2012/789525>.
- [39] F. Tian, X. Yang, Y. Shi, C. Jia, Y. Chen, Adsorptive desulfurization over hierarchical beta zeolite by alkaline treatment, *J. Nat. Gas Chem.* 21 (2012) 647–652, [http://dx.doi.org/10.1016/S1003-9953\(11\)60414-3](http://dx.doi.org/10.1016/S1003-9953(11)60414-3).
- [40] X. Meng, G. Qiu, G. Wang, Q. Cai, Y. Wang, Durable and regenerable mesoporous adsorbent for deep desulfurization of model jet fuel, *Fuel Process. Technol.* 111 (2013) 78–85, <http://dx.doi.org/10.1016/j.fuproc.2013.02.002>.
- [41] H. Chen, Y. Wang, F.H. Yang, R.T. Yang, Desulfurization of high-sulfur jet fuel by mesoporous  $\pi$ -complexation adsorbents, *Chem. Eng. Sci.* 64 (2009) 5240–5246, <http://dx.doi.org/10.1016/j.ces.2009.08.031>.
- [42] W. Li, Q. Liu, J. Xing, H. Gao, X. Xiong, Y. Li, et al., High-efficiency desulfurization by adsorption with mesoporous aluminosilicates, *AIChE J.* 53 (2007) 3263–3268, <http://dx.doi.org/10.1002/aic.11319>.
- [43] A. Takahashi, F.H. Yang, R.T. Yang, New sorbents for desulfurization by  $\pi$ -complexation: thiophene/benzene adsorption, *Ind. Eng. Chem. Res.* 41 (2002) 2487–2496, <http://dx.doi.org/10.1021/ie0109657>.
- [44] R.T. Yang, A.J. Hernández-Maldonado, F.H. Yang, Desulfurization of transportation fuels with zeolites under ambient conditions, *Science* 301 (2003) 79–81, <http://dx.doi.org/10.1126/science.1085088>.
- [45] A.J. Hernández-Maldonado, R.T. Yang, Desulfurization of diesel fuels via  $\pi$ -complexation with nickel(II)-exchanged X- and Y-zeolites, *Ind. Eng. Chem. Res.* 43 (2004) 1081–1089, <http://dx.doi.org/10.1021/le034206v>.
- [46] A.J. Hernández-Maldonado, R.T. Yang, Desulfurization of commercial liquid fuels by selective adsorption via  $\pi$ -complexation with Cu(I)-Y zeolite, *Ind. Eng. Chem. Res.* 42 (2003) 3103–3110, <http://dx.doi.org/10.1021/ie0301132>.
- [47] A.J. Hernández-Maldonado, R.T. Yang, Desulfurization of diesel fuels by adsorption via  $\pi$ -complexation with vapor-phase exchanged Cu(I)–Y zeolites, *J. Am. Chem. Soc.* 126 (2004) 992–993, <http://dx.doi.org/10.1021/ja039304m>.
- [48] X. Ma, S. Velu, J.H. Kim, C. Song, Deep desulfurization of gasoline by selective adsorption over solid adsorbents and impact of analytical methods on ppm-level sulfur quantification for fuel cell applications, *Appl. Catal. B Environ.* 56 (2005) 137–147, <http://dx.doi.org/10.1016/j.apcatb.2004.08.013>.
- [49] J.H. Kim, X. Ma, A. Zhou, C. Song, Ultra-deep desulfurization and denitrogenation of diesel fuel by selective adsorption over three different adsorbents: a study on adsorptive selectivity and mechanism, *Catal. Today* 111 (2006) 74–83, <http://dx.doi.org/10.1016/j.cattod.2005.10.017>.
- [50] M. Xue, R. Chitrakar, K. Sakane, T. Hirotsu, K. Ooi, Y. Yoshimura, et al., Preparation of cerium-loaded Y-zeolites for removal of organic sulfur compounds from hydrodesulfurized gasoline and diesel oil, *J. Colloid Interface Sci.* 298 (2006) 535–542, <http://dx.doi.org/10.1016/j.jcis.2005.12.051>.
- [51] L. Lin, Y. Zhang, H. Zhang, F. Lu, Adsorption and solvent desorption behavior of ion-exchanged modified Y zeolites for sulfur removal and for fuel cell applications, *J. Colloid Interface Sci.* 360 (2011) 753–759, <http://dx.doi.org/10.1016/j.jcis.2011.04.075>.
- [52] F. Tian, W. Wu, Z. Jiang, C. Liang, Y. Yang, P. Ying, et al., The study of thiophene adsorption onto La(III)-exchanged zeolite NaY by FT-IR spectroscopy, *J. Colloid Interface Sci.* 301 (2006) 395–401, <http://dx.doi.org/10.1016/j.jcis.2006.05.017>.
- [53] S. Nuntang, P. Prassasarakich, C. Ngamcharussrivichai, Comparative study on adsorptive removal of thiophenic sulfurs over Y and USY zeolites, *Ind. Eng. Chem. Res.* 47 (2008) 7405–7413, <http://dx.doi.org/10.1021/ie701785s>.
- [54] Y. Wang, R.T. Yang, Desulfurization of liquid fuels by adsorption on carbon-based sorbents and ultrasound-assisted sorbent regeneration, *Langmuir* 23 (2007) 3825–3831, <http://dx.doi.org/10.1021/la063364z>.
- [55] K.X. Lee, J.A. Valla, Investigation of bifunctional zeolites for the adsorptive desulfurization of fuels, *Appl. Catal. B Environ.* 201 (2017) 359–369, <http://dx.doi.org/10.1016/j.apcatb.2016.08.018>.
- [56] J. Wang, F. Xu, W.J. Xie, Z.J. Mei, Q.Z. Zhang, J. Cai, et al., The enhanced adsorption of dibenzothiophene onto cerium/nickel-exchanged zeolite Y, *J. Hazard. Mater.* 163 (2009) 538–543, <http://dx.doi.org/10.1016/j.jhazmat.2008.07.027>.
- [57] H. Song, Y. Chang, X. Wan, M. Dai, H. Song, Z. Jin, Equilibrium, Kinetic, and Thermodynamic Studies on Adsorptive Desulfurization onto Cu I Ce IV Y Zeolite, (2014).
- [58] H. Song, Y. Chang, H. Song, Deep adsorptive desulfurization over Cu, Ce bimetal ion-exchanged Y-typed molecule sieve, *Adsorption* 22 (2016) 139–150, <http://dx.doi.org/10.1007/s10450-015-9731-3>.
- [59] J. García-Martínez, M. Johnson, J. Valla, K. Li, J.Y. Ying, Mesosstructured zeolite Y—high hydrothermal stability and superior FCC catalytic performance, *Catal. Sci. Technol.* 2 (2012) 987, <http://dx.doi.org/10.1039/c2cy00309k>.
- [60] J.H. Shan, X.Q. Liu, L.B. Sun, R. Cui, Cu-Ce bimetal ion-exchanged Y zeolites for selective adsorption of thiophenic sulfur, *Energy Fuels* 22 (2008) 3955–3959, <http://dx.doi.org/10.1021/ef800296n>.
- [61] V.Y. Borovkov, M. Jiang, Y. Fu, Investigation of copper carbonyl species formed upon CO adsorption on copper-exchanged zeolites by diffuse reflectance FTIR, *J. Phys. Chem. B* 103 (1999) 5010–5019, <http://dx.doi.org/10.1021/jp984727+>.
- [62] J.F. Tempère, F. Bozon-Verduraz, D. Delafosse, A kinetic study of the oxidation of cerium ions in an X zeolite, *Mater. Res. Bull.* 12 (1977) 871–879, [http://dx.doi.org/10.1016/0025-5408\(77\)90098-8](http://dx.doi.org/10.1016/0025-5408(77)90098-8).
- [63] M. Sources, F. Rule, Environmental protection agency control of hazardous air pollutants from mobile sources; final rule, *Fed. Regist.* (2007) 72.
- [64] L.C. Marr, T.W. Kirchstetter, R.A. Harley, A.H. Miguel, S.V. Hering, S.K. Hammond, Characterization of polycyclic aromatic hydrocarbons in motor vehicle fuels and exhaust emissions, *Environ. Sci. Technol.* 33 (1999) 3091–3099, <http://dx.doi.org/10.1021/es9812271>.
- [65] J.-Y. Chin, S.A. Batterman, VOC composition of current motor vehicle fuels and vapors, and collinearly analyses for receptor modeling, *Chemosphere* 86 (2012) 951–958, <http://dx.doi.org/10.1016/j.chemosphere.2011.11.017>.
- [66] Y. Li, F.H. Yang, G. Qi, R.T. Yang, Effects of oxygenates and moisture on adsorptive desulfurization of liquid fuels with Cu(I)Y zeolite, *Catal. Today* 116 (2006) 512–518, <http://dx.doi.org/10.1016/j.cattod.2006.06.037>.
- [67] F.C. Meunier, L. Domokos, K. Seshan, J.A. Lercher, In situ IR study of the nature and mobility of sorbed species on H-FER during but-1-ene isomerization, *J. Catal.* 211 (2002) 366–378, [http://dx.doi.org/10.1016/S0021-9517\(02\)93703-6](http://dx.doi.org/10.1016/S0021-9517(02)93703-6).
- [68] T. Meng, N. Ren, Z. Ma, Silicalite-1@Cu-ZSM-5 core-shell catalyst for N<sub>2</sub>O decomposition, *J. Mol. Catal. A Chem.* 404–405 (2015) 233–239, <http://dx.doi.org/10.1016/j.molcata.2015.05.006>.
- [69] Y.S. Bi, G.Y. Dang, X.H. Zhao, X.F. Meng, H.J. Lu, J.T. Jin, Preparation, characterization and catalytic properties of Pd-Fe-zeolite and Pd-Ce-zeolite composite catalysts, *J. Hazard. Mater.* 229–230 (2012) 245–250, <http://dx.doi.org/10.1016/j.jhazmat.2012.05.101>.
- [70] H. Song, H. Song, X. Wan, M. Dai, J. Zhang, F. Li, Deep desulfurization of model gasoline by selective adsorption over Cu-Ce bimetal ion-exchanged Y zeolite, *Fuel Process. Technol.* 116 (2013) 52–62, <http://dx.doi.org/10.1016/j.fuproc.2013.04.017>.
- [71] F. Tian, Q. Shen, Z. Fu, Y. Wu, C. Jia, Enhanced adsorption desulfurization performance over hierarchically structured zeolite Y, *Fuel process. Technol.* 128 (2014) 176–182, <http://dx.doi.org/10.1016/j.fuproc.2014.07.018>.
- [72] M. Jiang, F.T.T. Ng, Adsorption of benzothiophene on Y zeolites investigated by infrared spectroscopy and flow calorimetry, *Catal. Today* 116 (2006) 530–536, <http://dx.doi.org/10.1016/j.cattod.2006.06.034>.
- [73] H. Wang, L. Song, H. Jiang, J. Xu, L. Jin, X. Zhang, et al., Effects of olefin on adsorptive desulfurization of gasoline over Ce(IV)Y zeolites, *Fuel Process. Technol.*

- 90 (2009) 835–838, <http://dx.doi.org/10.1016/j.fuproc.2009.03.004>.
- [74] G.S. Foo, A.K. Rogers, M.M. Yung, C. Sievers, Steric effect and evolution of surface species in the hydrodeoxygenation of bio-oil model compounds over Pt/HBEA, *ACS Catal.* 6 (2016) 1292–1307, <http://dx.doi.org/10.1021/acscatal.5b02684>.
- [75] Y. Zu, Y. Qin, X. Gao, H. Liu, X. Zhang, J. Zhang, et al., Insight into the correlation between the adsorption-transformation behaviors of methylthiophenes and the active sites of zeolites Y, *Appl. Catal. B Environ.* 203 (2017) 96–107, <http://dx.doi.org/10.1016/j.apcatb.2016.10.008>.
- [76] H. Song, X. Cui, H. Song, H. Gao, F. Li, Characteristic and adsorption desulfurization performance of Ag–Ce bimetal ion-exchanged Y zeolite, *Ind. Eng. Chem. Res.* 53 (2014) 14552–14557, <http://dx.doi.org/10.1021/ie404362f>.
- [77] L. Duan, X. Gao, X. Meng, H. Zhang, Q. Wang, Y. Qin, et al., Adsorption, Co-adsorption, and reactions of sulfur compounds, aromatics, olefins over Ce-exchanged y zeolite, *J. Phys. Chem. C* 116 (2012) 25748–25756, <http://dx.doi.org/10.1021/jp303040m>.
- [78] B. Thomas, S. Sugunan, Effect of rare earth metal ions on the structural and textural properties of NaFAU-Y zeolite and vapour phase alkylation of benzene with 1-octene, *Indian J. Chem. Technol.* 12 (2005) 676–688.
- [79] M.A. Larrubia, A. Gutiérrez-Alejandre, J. Ramrez, G. Busca, A FT-IR study of the adsorption of indole, carbazole, benzothiophene, dibenzothiophene and 4,6-di-benzothiophene over solid adsorbents and catalysts, *Appl. Catal. A Gen.* 224 (2002) 167–178, [http://dx.doi.org/10.1016/S0926-860X\(01\)00769-4](http://dx.doi.org/10.1016/S0926-860X(01)00769-4).
- [80] L. Wang, Z. Sun, Y. Ding, Y. Chen, Q. Li, M. Xu, et al., A theoretical study of thiophenic compounds adsorption on cation-exchanged y zeolites, *Appl. Surf. Sci.* 257 (2011) 7539–7544, <http://dx.doi.org/10.1016/j.apsusc.2011.03.115>.
- [81] J.K. Thomas, K. Gunda, P. Rehbein, F.T.T. Ng, Flow calorimetry and adsorption study of dibenzothiophene, quinoline and naphthalene over modified Y zeolites, *Appl. Catal. B Environ.* 94 (2010) 225–233, <http://dx.doi.org/10.1016/j.apcatb.2009.11.012>.
- [82] A. Gutiérrez-Alejandre, M.A. Larrubia, J. Ramírez, G. Busca, FT-IR evidence of the interaction of benzothiophene with the hydroxyl groups of H-MFI and H-MOR zeolites, *Vib. Spectrosc.* 41 (2006) 42–47, <http://dx.doi.org/10.1016/j.vibspec.2005.12.008>.
- [83] E. Vilarrasa-García, D.C.S. Azevedo, P. Braos-García, A. Infantes-Molina, C.L. Cavalcante, J. Jiménez-Jiménez, et al., Synthesis and characterization of metal-supported mesoporous silicas applied to the adsorption of benzothiophene, *Adsorpt. Sci. Technol.* 29 (2012) 691–704, <http://dx.doi.org/10.1260/0263-6174.29.7.691>.
- [84] Y. Yang, N. Burke, J. Zhang, S. Huang, S. Lim, Y. Zhu, Influence of charge compensating cations on propane adsorption in X zeolites: experimental measurement and mathematical modeling, *RSC Adv.* 4 (2014) 7279, <http://dx.doi.org/10.1039/c3ra46987e>.
- [85] Z.R. Yelebe, B.Z. Yelebe, R.J. Samuel, *Contaminants from Industrial Wastewater* 5 (2013).
- [86] X. Gao, W. Geng, H. Zhang, X. Zhao, X. Yao, Thiophenic compounds adsorption on Na(Y) and rare earth exchanged Y zeolites: a density functional theory study, *J. Mol. Model.* 19 (2013) 4789–4795, <http://dx.doi.org/10.1007/s00894-013-1954-1>.
- [87] T.A. Egerton, F.S. Stone, Adsorption of carbon monoxide by zeolite Y exchanged with different cations, *J. Chem. Soc. Faraday Trans. 1 Phys. Chem. Condens. Ph.* 69 (1973) 22, <http://dx.doi.org/10.1039/f19736900022>.
- [88] S. Djemel, M.-F. Guilleux, J. Jeanjean, J.F. Tempere, D. Delafosse, Effect of Ce<sup>3+</sup> ions exchanged in NiX zeolites on the location and reducibility of Ni<sup>2+</sup> ions and on the stabilization of a highly dispersed metallic nickel, *J. Chem. Soc. Faraday Trans. 1 Phys. Chem. Condens. Ph.* 78 (1982) 835, <http://dx.doi.org/10.1039/f19827800835>.
- [89] G. Turnes Palomino, S. Bordiga, a. Zecchina, G.L. Marra, C. Lamberti, XRD, XAS, and IR characterization of copper-exchanged Y zeolite, *J. Phys. Chem. B* 104 (2000) 8641–8651, <http://dx.doi.org/10.1021/jp000584r>.
- [90] G. Turnes Palomino, S. Bordiga, C. Lamberti, a. Zecchina, C. Otero Areán, Vibrational and Optical Spectroscopic Studies on Copper-Exchanged Ferrierite, (2002), pp. 199–206, [http://dx.doi.org/10.1016/S0167-2991\(02\)80029-5](http://dx.doi.org/10.1016/S0167-2991(02)80029-5).
- [91] J. Jiang, F.T.T. Ng, Production of low sulfur diesel fuel via adsorption: an equilibrium and kinetic study on the adsorption of dibenzothiophene onto NaY zeolite, *Adsorption* 16 (2010) 549–558, <http://dx.doi.org/10.1007/s10450-010-9259-5>.
- [92] L. Wang, B. Sun, F.H. Yang, R.T. Yang, Effects of aromatics on desulfurization of liquid fuel by π-complexation and carbon adsorbents, *Chem. Eng. Sci.* 73 (2012) 208–217, <http://dx.doi.org/10.1016/j.ces.2012.01.056>.
- [93] J. Fujiki, E. Furuya, Density functional theory study of adsorption of benzothiophene and naphthalene on silica gel, *Fuel* 164 (2016) 180–185, <http://dx.doi.org/10.1016/j.fuel.2015.10.013>.